



Pre-test Numerical Modelling of Stainless Steel and Hybrid Links

Anna Ene^(✉)  and Aurel Stratan 

Politehnica University Timisoara, Timișoara, Romania
anna.ene@student.upt.ro, aurel.stratan@upt.ro

Abstract. Eccentrically braced steel frames have of good balance between lateral stiffness, strength and ductility, and therefore are often preferred as a seismic-resistant system. Replaceable bolted links and a dual structural configuration, consisting of eccentrically braced and moment resisting frames was proposed in the past for enhancing the structural system with re-centering capability. Further enhancement of the seismic performance is sought through adopting stainless steel links for increasing link ductility, and high-strength steel, which could reduce the link overstrength. To this end, a series of pre-test numerical investigations are performed on several link made of mild, stainless, and high-strength steel. Short links are adopted, which dissipate the seismic energy by yielding essentially in shear. Obtained numerical results indicate that existing design criteria are inappropriate for stainless and hybrid links. A new and more general criteria for the normalized link length is proposed, which explicitly accounts for the steel properties of the flanges and the web. Finite element simulations on several homogeneous and hybrid links made of mild, stainless and high strength steel proves and appropriate behaviour of links designed using the new criterion.

Keywords: Hybrid links · Stainless steel · High-strength steel · Normalized length · Ductility

1 Introduction

Eccentrically braced frames (EBFs) with links acting as dissipative members were initially proposed in the early 1970s by a group of Japanese researchers [1]. The structural system was further investigated by researchers from the USA [2, 3], where the first design guidelines for EBF structures were developed. The eccentrically braced frames have proven to be a highly ductile solution, which can isolate plastic deformations in structural fuses (links) and provide a stable and controlled energy dissipation. Lately, replaceable bolted links for eccentrically braced were proposed [4]. Implemented within a dual structural system, composed of EBFs with replaceable links and moment resisting frames (MRFs), a re-centering system is obtained, which brings the advantage of easy repair after a major earthquake [5]. Past researches pointed out the need to adopt very short replaceable bolted links to allow capacity design of the connection, with certain outcomes: large plastic deformation demands in links and large link overstrength [4, 6]. Recently, aiming to improve link performance, stainless steel links were numerically investigated [7].

Use of austenitic stainless steels for links targets exploiting the excellent ductility of stainless steel, with elongation at fracture of 40–45% [8], compared to the mild carbon steel, with elongation of 20–26% [9]. Additionally, austenitic stainless steel has the advantage of very good toughness at low temperatures.

Despite the benefit of a higher ductility of the stainless steel, it is also characterized by large strain hardening, which may generate large overstrength in links. This leads to large resistance demands in non-dissipative components of the EBF, and, consequently, higher costs of the structure. Hybrid links with stainless steel web and high-strength steel flanges could potentially reduce link overstrength, due to lower contribution of flanges.

Performance of stainless and hybrid links will be investigated experimentally. This paper aims at assessing the efficiency of these solutions via pre-test numerical analysis of three types of short links: MCS - the reference, homogeneous mild-carbon steel (S235) link; SS - homogeneous stainless steel (1.4404) link; SS+HSS - hybrid (1.4404 + S690) link. The numerical simulations were performed within Abaqus/CAE software package.

2 Design of the Links

A re-centring dual structure having 3 storeys, 3 spans and 5 bays, and located in a seismic zone with a peak ground acceleration of $a_g = 0,25$ g was designed for DCH ductility class according to EN 1998-1:2004 [10]. The lateral force resisting system consists of EBFs meant to ensure the concentration of seismic energy in the dissipative fuses, and MRFs meant to provide the necessary re-centring capability. Short links were designed as replaceable dissipative components.

Seismic design codes [10] classify the links as short using Eq. (1), based on a criterion developed by [2], which assumes the equilibrium between the maximum moment M_p (after strain hardening) and the maximum shear force V_p developed by the link:

$$e \leq e_s = \frac{2(1,2 \cdot M_p)}{1,5 \cdot V_p} = \frac{1,6M_p}{V_p} = \frac{\rho \cdot M_p}{V_p} \quad (1)$$

where M_p is the link plastic moment, V_p is the link plastic shear resistance, and ρ is the normalized length. The resulting link cross-sections are presented in Table 1.

Table 1. Link dimensions following the initial code-based design

Link type	Link length (e), mm	Limit for short links (e_s), mm	Height, mm	Flange width, mm	Flange thickness, mm	Web thickness, mm
MCS	450	485	240	140	10	8
SS	450	450,3	250	130	10	8
SS+HSS	450	456,3	240	70	6	8

3 Numerical Model

3.1 Calibration of the Numerical Model

The numerical model of the link was calibrated on past experimental tests performed on mild carbon steel links [11]. The finite element model developed using ABAQUS software includes both the link and the experimental rig (Fig. 1). The frame was modelled using beam and truss elements, while the link using shell elements (S4R element type, a 4-node general-purpose shell with reduced integration and hourglass control). The imposed boundary conditions (out-of-plane and torsional restraints) aimed at reproducing, as closely as possible, the experimental setup. The results of FEM analysis, in terms of link shear force (V) and deformation (γ), show a good agreement with the experimental response (Fig. 2).

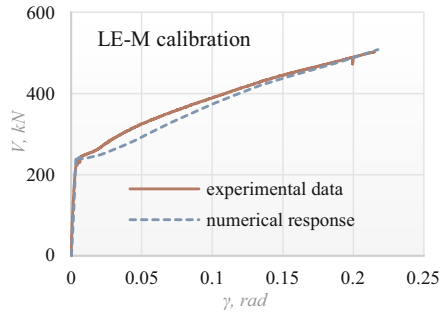
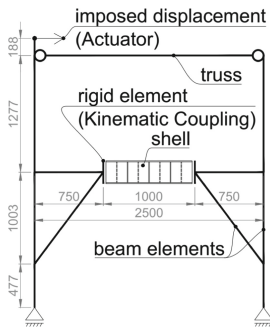


Fig. 1. FEM model of the test setup

Fig. 2. Numerical vs. experimental response curves

3.2 Calibration of the Constitutive Models for Steel

The accuracy of numerical simulations on links depends on the reliability of the constitutive models of the corresponding materials. As already mentioned, three grades of steel have been considered in this study: mild carbon steel S235 J2, stainless steel 1.4404 and high-strength steel S690 QL. Since the results presented in this paper concern pre-test numerical investigations, material models were developed on the basis of nominal properties of steel (minimum yield strength R_{eH} , 0.2% proof strength $R_{p0.2}$, tensile strength R_m , elongation after fracture A), described in Table 2.

Table 2. Nominal mechanical properties for different steel grades

Steel grade	Standard	R_{eH} [MPa]	$R_{p0.2}$ [MPa]	R_m [MPa]	A [% min.]
S235 J2	EN 10025-2:2004	235		510	24
1.4404 (AISI 316L)	EN 10088-4:2009		220	670	40
S690 QL	EN 10025-6:2004	690		940	14

For specified mild carbon steel was adopted a 4-stages engineering stress-strain curve based on calibrated polynomial relationships, while for stainless steel and high-strength steel were adopted Ramberg-Osgood models [12]. Up to the ultimate

stress, the true stress-strain relationships were obtained from the engineering ones using the following formulas: $\sigma_{true} = \sigma(1 + \epsilon)$, $\epsilon_{true} = \ln(1 + \epsilon)$ [13]. In the post-necking range the true stress-strain relationships were obtained using a trial and error approach, based on numerical simulation of the tensile tests on steel coupons, using shell elements with the size of approximately 10 mm, same as in link models. The softening part of the true-stress – true strain curves are meant to account in an approximate manner of the material failure, and the values corresponding to engineering fracture strain were pointed out on the true stress-strain diagrams (Fig. 3).

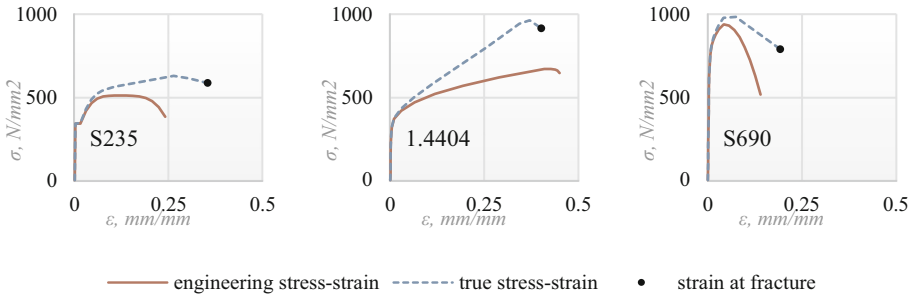


Fig. 3. Engineering and true stress-strain curves for the considered materials

It is interesting to note that the true strain at fracture of stainless steel is not significantly higher than then one of mild-carbon steel, unlike the engineering one.

3.3 Modelling of Links

To reduce computational time, an isolated link was modelled using 4-node shell elements with reduced integration (S4R) available in the ABAQUS element library. In particular, for the sake of consistency, the size of finite elements of the link matches the mesh size of the tensile test coupons used to calibrate material model (approximately 10 × 10 mm), in order to rule out any mesh-sensitive discordance. End cross-sections of the link model were tied with kinematic constraints to reference points RP1 and RP2. One end of the link was fully restrained, while a transverse displacement (U2) was applied to the other one. The link was unrestrained axially (Fig. 4).

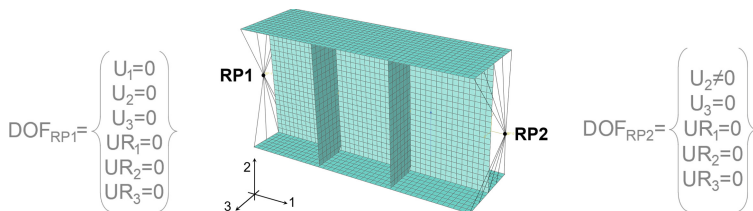


Fig. 4. Boundary conditions of the numerical model of the links

Global imperfections were modelled by restraining out-of-plane translations along the web panels and applying a pressure load on the link web to obtain a deflection equal to the minimum side length divided by 200.

4 Results and Discussion

The three link models (MCS, SS and SS+HSS) with the geometrical characteristics described in Table 1, and modelled as described in Sects. 3.2 and 3.3, were analysed under monotonic loading. Figure 5 shows the deformed shape and the equivalent plastic strains (PEEQ) at a link rotation corresponding to attainment of the steel fracture strain, see Fig. 8a. It can be observed that the stainless steel (SS) and hybrid (SS+HSS) links exhibit a behaviour characterised by larger plastic engagement of the flanges, in comparison with mild carbon steel link (MCS). Non-uniform yielding of the web, with larger plastic deformations in the first and last web panels are visible for the SS link. Considerably larger plastic strains in the flanges than in the web could be observed for the hybrid (SS+HSS) link. Both phenomena are attributed to inappropriate design criteria for short links for stainless and hybrid links. It can be concluded the code criterion from Eq. (1) is not appropriate for stainless steel and hybrid links. A more general criterion is suggested by the authors, which explicitly accounts of the strain hardening and overstrength due to random material variability. Thus, the normalised link length ρ is obtained using Eq. (2) as:

$$\rho = 2 \cdot \frac{\omega_{sh,M} \cdot \omega_{rm,f}}{\omega_{sh,V} \cdot \omega_{rm,w}} \quad (2)$$

where $\omega_{sh,M}$ is the hardening factor due to flexural action; $\omega_{sh,V}$ is the hardening factor due to shear action; $\omega_{rm,f}$ is the material overstrength of the flange; $\omega_{rm,w}$ is the material overstrength of the web.

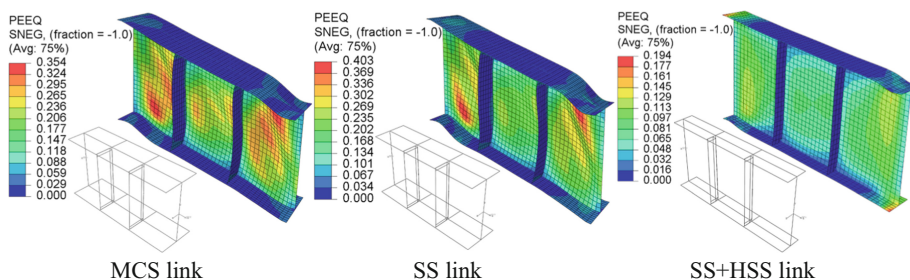


Fig. 5. Equivalent plastic strain distribution at fracture

The stainless steel and hybrid links were redesigned according to the improved formulation of the normalised link length. Assumed values of overstrength factors (ω_{sh} and ω_{rm}), as well as the new values of normalized length and re-designed dimensions of the cross-sections are presented in Table 3.

Table 3. Recalculated normalized length and redesign for 3 link types

Link type	$\omega_{sh,M}$	$\omega_{rm,f}$	$\omega_{sh,V}$	$\omega_{rm,w}$	ρ	Re-designed cross-section
MCS	1.2	1.45	1.5	1.45	1.6	240 × 140 × 10 × 8
SS	1.2	1.45	1.7	1.45	1.4	250 × 140 × 12 × 8
SS+HSS	1.05	1.05	1.7	1.45	0.9	250 × 80 × 10 × 8

Figure 6 shows the force-deformation curves and the equivalent plastic strains for the stainless steel and hybrid links, design using current code approach ($\rho = 1,6$) and redesigned using the proposed approach ($\rho = 1,4$ for stainless steel links, and $\rho = 0,9$ for hybrid ones). An increase in ductility and also a significantly more uniform strain distribution in the web could be noticed after redesign, which validates numerically the proposed formulation for the normalized link length ρ .

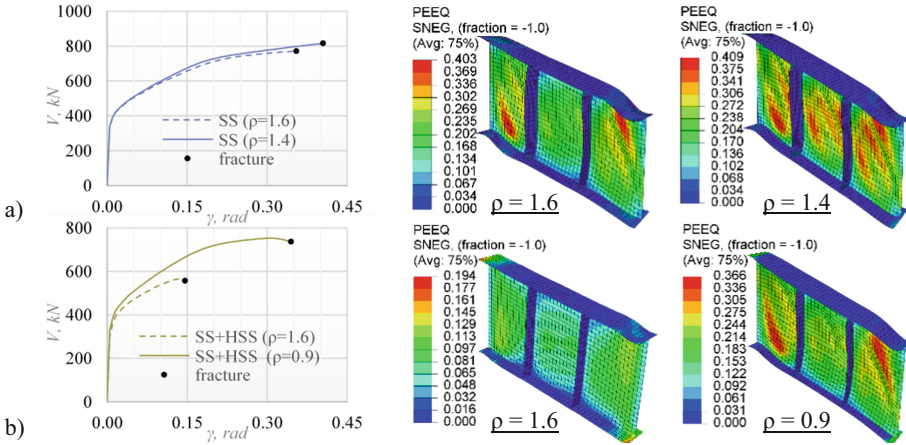


Fig. 6. Comparison between stress-strain curves and strain distribution mapping for initial and redesigned a) SS and b) SS+HSS links

Further numerical investigation concerns the influence of stiffeners on link behaviour. According to [10] for links with a depth less than 600 mm, stiffeners are required on one side only. As can be observed in Fig. 7, the strains are not uniformly distributed among the web panels in the case of the SS and SS+HSS links with one-sided stiffeners. By using double-sided stiffeners, they develop significantly more uniform strains.

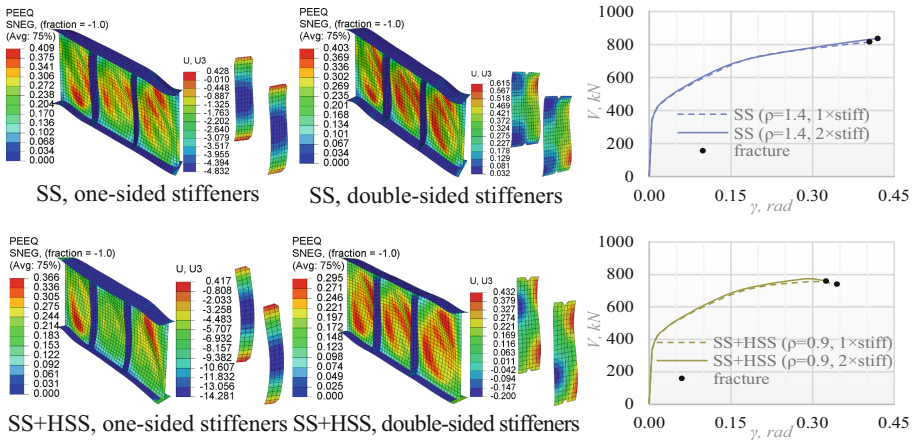


Fig. 7. Equivalent plastic strain, stress-strain curve and the out-of-plane deformations of the links with one-sided and two-sided stiffeners

Another argument that makes this solution reasonable is reducing the deformations of the stiffeners in the out-of-plane (with respect to the web) direction. The double-sided stiffeners are especially efficient (and even needed) for the hybrid links, as the out-of-plane deformations of the stiffeners reduced from 14,3 mm to 0,43 mm, and the equivalent plastic strains in the web decreased by 20% with respect to the sing-sided stiffener configuration, indicating a significant improvement in link behaviour.

Figure 8 compares links performance in terms ultimate link deformations, corresponding to attainment of fracture strains in the material. It can be observed that improved design criteria for stainless steel and hybrid links (new formulation of normalised link length and double stiffeners) improves ultimate link deformations. The effect new design criteria is especially important in case of the hybrid link. Different properties of the web and flange material (in terms of strain hardening and material overstrength) requires an adjusted criteria for normalised link length. On the other hand, high strength steel used for flanges leads to a quite slender out-of-plane link, which requires double-sided stiffeners.

Comparing the performance of mild carbon, stainless, and hybrid links with improved design (Fig. 8b), it can be observed that stainless steel link provides the largest ductility, though the increase over the mild carbon steel link (29%) is not proportional to the corresponding material properties (elongation at fracture, see Table 2). The increase of ductility of the stainless steel link comes though with a larger overstrength, which brings the disadvantage of larger strength demands on non-dissipative components of EBFs. The hybrid link, as intended, alleviates to some extent the large overstrength of stainless steel link, but has an ultimate deformation similar to the mild carbon steel link. Therefore, it does not show any obvious advantages over the former one.

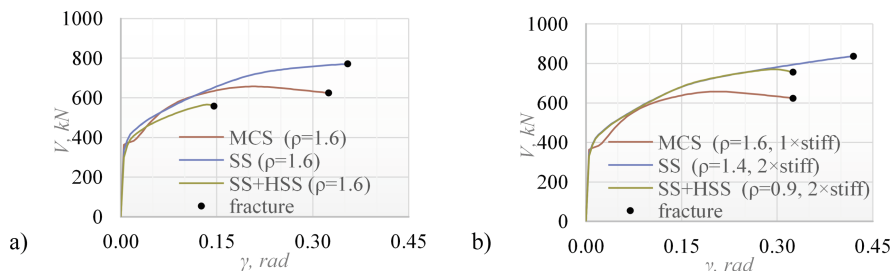


Fig. 8. Monotonic response in terms of moment-rotation curve of three link typologies: (a) code-designed links; (b) re-designed links

5 Conclusions

Stainless steel links were investigated numerically in this paper, in an effort to exploit the large ductility of stainless steel. Hybrid (stainless and high strength steel) links were also addressed with the tentative objective of keeping under control the overstrength of purely stainless steel links. Results indicate that code criteria for shear links are not appropriate for stainless, and especially hybrid (stainless and high strength) links.

Improved formulations for link normalised length ρ were proposed, that account explicitly and independently of the overstrength due to random material variability and of the strain hardening. On the other hand, single-sided stiffeners, as permitted by design codes for shallow links, were found inappropriate for hybrid cross-section, due to its rather large slenderness in the out-of-plane direction. Two-sided stiffeners significantly improved the performance of the hybrid links. The stainless steel link has larger ductility in comparison with the mild carbon steel one, though the improvement is not proportional to the material ductility. Hybrid links, at this point, does not bring any clear advantages over the other two alternatives. Future research will investigate the monotonic and cyclic performance of the three categories of links addressed in this study.

Acknowledgments. This work was supported by a grant of the Romanian Ministry of Education and Research, CCCDI - UEFISCDI, project number PN-III-P2-2.1-PED-2019-5427, within PNCDI III.

References

1. Fujimoto M, Aoyagi T, Ukai K, Wada A, Saito K (1972) Structural characteristics of eccentric k-braced frames. *Trans AIJ* 195:39–49
2. Manheim DN, Popov EP (1983) Plastic shear hinges in steel frames. *J Struct Eng* 109 (10):2404–2419
3. Kasai K, Popov EP (1986) General behavior of WF steel shear link beams. *J Struct Eng* 112 (2):362–382
4. Stratan A, Dubina D (2004) Bolted links for eccentrically braced steel frames. Presented at the connections in steel structures V
5. Dubina D, Stratan A, Dinu F (2008) Dual high-strength steel eccentrically braced frames with removable links. *Earthq Eng Struct Dyn* 37:1703–1720
6. Chesoa A, Stratan A, Dubina D (2018) Design implementation of re-centring dual eccentrically braced frames with removable links. *Soil Dyn Earthq Eng* 112:174–184
7. Chacón R, Vega A, Mirambell E (2019) Numerical study on stainless steel I-shaped links on eccentrically braced frames. *J Constr Steel Res* 159:67–80
8. EN 10088-4:2009. Stainless steels - Part 4: Technical delivery conditions for sheet/plate and strip of corrosion resisting steels for construction purposes
9. EN 10025-2:2004. Hot rolled products of structural steels - Part 2: Technical delivery conditions for non-alloy structural steels
10. EN 1998-1:2004. Eurocode 8: Design of structures for earthquake resistance - Part 1: General rules, seismic actions and rules for buildings
11. Chesoa A, Stratan A, Neagu C, Dubina D (2020) Experimental investigation of the length influence on removable links. In: *Proceedings IRF2020: 7th ICIRF*
12. prEN1993-1-14:2020. Eurocode 3: Design of steel structures - Part 1-14: Design assisted by finite element analysis
13. EN 1993-1-1:2005. Eurocode 3: Design of steel structures - Part 1-1: General rules and rules for buildings